The Summer Hydrography and Surface Circulation of the East Siberian Shelf Sea*

ANDREAS MÜNCHOW

Institute of Marine and Coastal Sciences, Rutgers–The State University, New Brunswick, New Jersey

THOMAS J. WEINGARTNER

Institute of Marine Science, University of Alaska, Fairbanks, Alaska

LEE W. COOPER

Environmental Sciences Division, Oak Ridge National Laboratory, Oak Ridge, Tennessee

(Manuscript received 12 May 1998, in final form 2 September 1998)

ABSTRACT

During the ice-free summer season in 1995 the authors deployed and subsequently tracked 39 surface drifters to test the hypothesis that the discharge from the Kolyma River forces a buoyancy-driven coastal current from the East Siberian Sea toward Bering Strait. The observed mean flow is statistically significant at the 95% level of confidence, but its direction contradicts their initial hypothesis. Instead of a coastally trapped eastward flow, the authors find a laterally sheared westward flow with maximum velocities offshore that correlate only weakly with the local winds. At a daily, wind-dominated timescale the drifter data reveal spatially coherent flows of up to 0.5 m s^{-1}. The Lagrangian autocorrelation scale is about 3 days and the Lagrangian eddy length scale reaches 40 km. This spatial scale exceeds the nearshore internal deformation radius by a factor of 3; however, it more closely corresponds to the internal deformation radius associated with the offshore ice edge. Bulk estimates of the horizontal mixing coefficient resemble typical values of isotropic open ocean dispersion at midlatitudes. Hydrographic observations and oxygen isotope ratios of seawater indicate a low proportion of riverine freshwater relative to sea ice melt in most areas of the East Siberian Sea except close to the Kolyma Delta. The observations require a reevaluation of the conceptual view of the summer surface circulation of the East Siberian Sea. Eastward buoyancy-driven coastal currents do not always form on this shelf despite large river discharge. Instead, ice melt waters of a retreating ice edge act as a line source of buoyancy that in 1995 forced a westward surface flow in the East Siberian Sea.

1. Introduction

During the aftermath of the Russian revolution the renowned oceanographer Harald Sverdrup spent three years aboard the sailing vessel *Maud* while it was trapped in the ice of the East Siberian Sea. The goal of this epic 1922 to 1924 expedition was to repeat Nansen's earlier drift on the *Fram* across the Arctic Ocean with the polar ice pack. The *Maud* failed to leave the vast shelf seas to the north of Siberia; however, the scientists aboard collected extensive salinity, temperature, and velocity data along the ship's ice bound drift (Sverdrup 1929). These data constituted the only readily accessible hydrographic information for the area until the military vessels USS *Barton* and USCGS *Northwind* surveyed the area within 3 nm of the Siberian coast at the height of the Cold War in 1962 and 1966. In 1995 the R/V *Alpha Helix* was the first U.S. research vessel to enter the East Siberian Sea. During this summer cruise we deployed 39 surface drifters in ice-free shelf waters while conducting hydrographic surveys in order to explore the influence of the Kolyma River on the shelf circulation. This study constituted the first oceanographic experiment in the East Siberian Sea after the Cold War. It was conducted in a spirit of international cooperation. For this spirit to prevail, however, we must remember the men, women, and children that earlier this century vanished in the Kolyma region (Conquest 1978).

Arctic shelf processes impact ice cover, thermohaline circulation, and biochemical budgets of the Arctic Ocean and adjacent seas (Björk 1989; Carmack 1990; Gawarkiewicz and Chapman 1995; Jones and Anderson

* Institute of Marine and Coastal Sciences Contribution Number 98-27.

Corresponding author address: Dr. Andreas Münchow, Inst. of Marine and Coastal Sciences, Rutgers–The State University, 71 Dudley Rd., New Brunswick, NJ 08901-8521.
E-mail: andreas@ahab.rutgers.edu

1986). For example, the salinity of the surface waters determines the amount of salt rejected from sea ice as it grows. The dense bottom water that is formed by these brines on shallow shelves maintains the halocline of the central Arctic basins (Aagaard et al. 1981). The supply of the halocline constitutes an important element in the global climate system because it insulates surface waters and thus the ice cover from the vertical heat flux of warmer waters at depth. Melling (1993) argues that shelf processes strongly influence dense water formation as they control the distribution and dispersal of freshwater from riverine discharges prior to winter freezing. More specifically, the removal of freshwater from the shelf decreases vertical stratification, increases surface salinity, and thus enhances the amount of brines produced on the shelf.

The wide continental shelves off Siberia receive large amounts of riverine freshwater (Aagaard and Carmack 1989) and sediments (Milliman and Meade 1983). The river inflow establishes strong vertical density gradients that inhibit vertical exchange. Schlosser et al. (1994) estimate that riverine freshwater resides about 2–5 years on Siberian shelves. Due to its remote and strategically sensitive location, however, few published oceanographic observations are available from the East Siberian Sea. Codispoti and Richards (1968) and Coachman and Rankin (1968) report hydrographic and spotty current observations from a summer survey of the East Siberian shelf and Long Strait, respectively. They find summer surface salinities below 15 psu in bands more than 200 km across the shelf near rivers that drain much of the northern Asian continent of freshwater.

The main objective of this study is to explore the shelf circulation in the East Siberian Sea during the summer season when the Kolyma River discharge constitutes a potentially important buoyancy forcing. Riverine waters always represent a lateral flux of mass and buoyancy that impacts the dynamics on the adjacent continental shelf. Yankovsky and Chapman (1997) and Garvine (1999) present elegant theories on the scales of buoyant plumes and buoyancy driven coastal currents. For typical Kolyma River discharge and geometric scales (discussed below), Yankovsky and Chapman (1997) predict a surface-advected plume that extends about 30–35 km across the shelf while Garvine (1999) predicts an alongshore extent of the coastal current of about 300–500 km. Both theories exclude ambient flows, wind-driven motions, and tidal currents.

The remote location, harsh environment, and largely unexplored physical oceanography of the Siberian shelf seas render comprehensive and focused process studies prohibitively expensive. Drifter studies offer an inexpensive and attractive alternative as they provide spatial and temporal information on the flow field (Davis 1991). The deployment of a large number of drifters, however, is essential to estimate statistically meaningful fields. Individual drifter trajectories may have appealing characteristics; however, they often lack significance in spatially and temporally variable fields (Regier and Stommel 1979). We here report for the first time on the density and surface velocity fields of the East Siberian Sea.

2. Study area and data sources

The East Siberian Sea constitutes a 1000-km long, 400-km wide, and 40-m deep shelf sea in the Arctic Ocean (Fig. 1). The New Siberian and Wrangel Islands at 140°E and 180° long are its boundaries with the Laptev Sea in the west and the Chukchi Sea in the east. Since our study area includes the date line, we subsequently present all maps with longitudes measured positive westward. The Kolyma Delta is then located at 200°W (160°E) long (Fig. 1). Annually averaged discharges from the Kolyma River into the East Siberian Sea vary from just below 2000 $m^3\ s^{-1}$ to almost 5000 $m^3\ s^{-1}$ (Fig. 2); the climatological mean from 1936 to 1996 is about 3160 $m^3\ s^{-1}$ (R. B. Lammers 1998, personal communication). The annually averaged discharge for 1995 was 3080 $m^3\ s^{-1}$, close to its climatological mean. The freshwater discharge into the East Siberian Sea is highly seasonal with more than 90% of the annual discharge occurring between June and September (Fig. 2). It increases from a May average of less than 1000 $m^3\ s^{-1}$ to a June average of more than 10 000 $m^3\ s^{-1}$. Monthly averaged discharge during the winter from November through April is less than 500 $m^3\ s^{-1}$. The Lena River to the west, too, contributes to the freshwater budget of the East Siberian Sea. Its peak freshwater discharge can exceed 100 000 $m^3\ s^{-1}$ in June (Létolle et al. 1993), which is about half the peak discharge of the Amazon River.

In the summer of 1995, we deployed 39 surface drifters manufactured to our specifications by Horizon Marine Inc., Marion, Massachusetts. Each drifter consists of a cylindrical body and a separate drogue. A 1-m high, sturdy cylinder encloses batteries, electronic circuit, ARGOS radio transmitter, and antenna. A separate 2-m long ''holey sock'' drogue is centered 2 m below a surface buoyancy element. The drogue is tethered to the cylindrical drifter by a 3-m long line. The drifters differ from the WOCE holey sock drifter because both the drogue and the surface elements are smaller. The ratio $R = \Sigma_D/\Sigma_S$ between drag coefficient times the frontal area of the drogue (Σ_D) and the drag coefficients times the frontal areas of the surface elements (Σ_S) is about 26 for our drifter while it is about 40 for the WOCE drifter (Niiler et al. 1995). Hence, our drifters have a slip that is about 50% larger than that of a WOCE drifter, that is, we claim that slip velocities are less than 0.015 $m\ s^{-1}$ at 10 $m\ s^{-1}$ winds. The drifters were programmed to collect data continuously during the 3-month-long summer season while in the winter, when they tracked ice motions, they collected data 8 hours daily. ARGOS transmits drifter locations almost hourly in our study area. We interpolate the irregular position data with a cubic spline to a time series with a constant time step

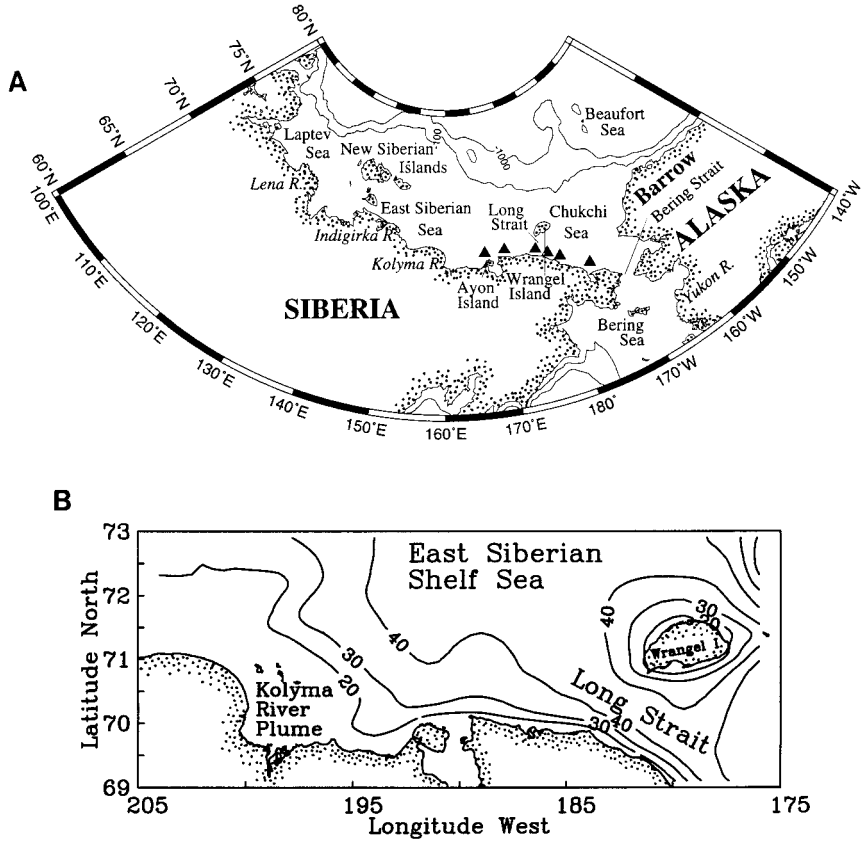

FIG. 1. Maps of the study area showing (a) the western Arctic along with the 100-m and 1000-m isobaths indicating the shelf break and (b) the western portion of the East Siberian Sea including Long Strait and Wrangel Island near the date line. The triangles in (a) indicate deployment locations of drifter clusters.

of 6 h. Tidal currents (not shown) are generally less than 0.05 m s^{-1}; only near Wrangel Island are they larger than 0.1 m s^{-1} (Kowalik and Proshutinsky 1994). Nevertheless, a Lanczos filter removes tidal and inertial motions from the interpolated time series of position. The filter passes less than 10% and more than 90% of the signal at periods near 30 and 60 h, respectively; the half-power point is at 40 h. We use centered differences to estimate velocity components from the interpolated, filtered, and subsampled drifter position data. Here we present data during the ice-free summer season of 1995 collected from yearday 235 (24 August) to 290 (17 October).

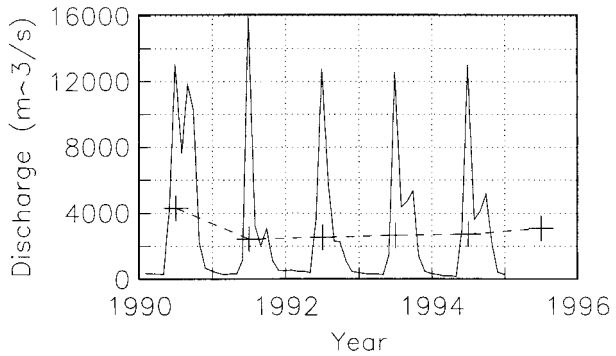

FIG. 2. Kolyma River discharge. The dotted line with "+" symbols shows the annual mean discharge from 1990 to 1996 while the solid line indicates monthly mean discharge from 1990 to 1994. Note that the 1995 annual mean discharge is similar to the preceeding years.

All drifters were deployed in ice-free waters between 5 and 50 km from the coast. Figures 3a and 3b show drifter deployment locations in August and September 1995, respectively. Also shown is the approximate location of the ice edge, which we digitized from weekly ice maps provided by the National Oceanic and Atmospheric Administration/Navy Joint National Ice Center. During the drifter deployments in the East Siberian Sea the ice edge retreated from about 70.5°N to 71.5°N lat within about 2 weeks. This ice distribution indicates an exceptionally light ice year with much melting. The freshwater input due to melting 1 m of ice over the 600 $\times$ 200 km^2 ice-free area of the western East Siberian Sea in 1995 is similar to the freshwater it receives from the Kolyma River (Fig. 2).

We estimate the wind field from sea level pressure

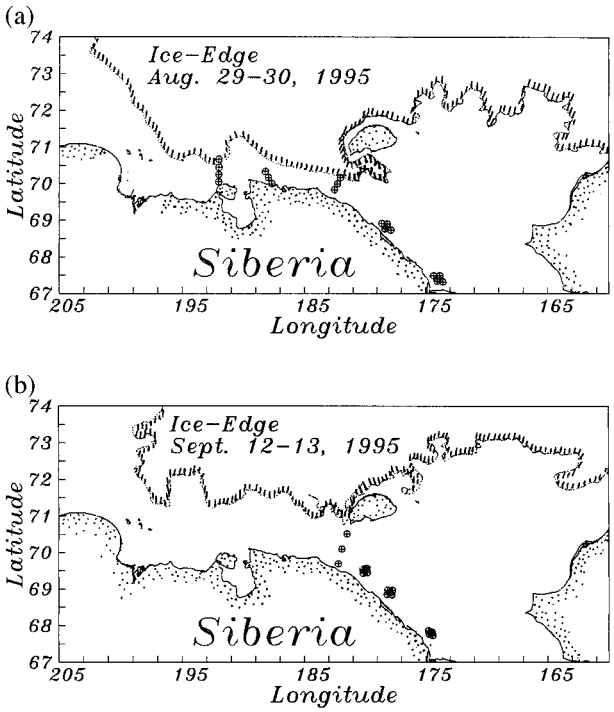

FIG. 3. Drifter deployment locations in (a) Aug and (b) Sep 1995 along with the location of the ice edge at the time of drifter deployments.

forecasts of the U.S. Navy Fleet Numerical Meteorological and Oceanographic Center models to calculate geostrophic winds. Following Overland and Colony (1994), we correct for speed and direction to account for the frictional effects of the atmospheric Ekman layer. Figure 4 shows the time series of wind velocities at locations near the Kolyma River (Fig. 4a), Wrangel Island (Fig. 4b), and Bering Strait (Fig. 4c). The data are low-pass filtered with the filter described above. Winds prior to the experiment (not shown) near the Kolyma River and Long Strait were from the northeast and east and generally weak (<5 m s^{-1}). During the subsequent drifter deployment, winds reached modest strength (<10 m s^{-1}) throughout the region with magnitudes diminishing westward. During the first 3 weeks in September (yearday 242–261) winds originated from the easterly quadrant near the Kolyma River and Long Strait, but in Bering Strait they originated from the northern quadrant. In October (yearday 270) winds strengthened and became more northerly over the Chukchi Sea including Long Strait but were weaker and from an easterly direction near the Kolyma River. A weak upwelling-favorable wind component appears over a portion of our study area.

CTD and bottle casts were taken at 76 locations throughout the study area with a SeaBird 911 instrument. Pre- and postcruise sensor calibrations and comparisons with bottle salinities indicate that the accuracy for salinity, temperature, and pressure are better than 0.01 psu, 0.01°C, and 1 db, respectively. In the following discussion we will use salinity synonymously with density because at low temperatures and in shallow water the contributions of temperature and pressure to density are negligible. Salinity is furthermore an excellent tracer of both ice melt and river waters, however, in order to distinguish between these two freshwater sources, we need another tracer such as stable oxygen isotope ratios (Strain and Tan 1993).

Stable oxygen isotope ratios of seawater ($H_2{}^{18}O/H_2{}^{16}O$) have been used as a conservative tracer of water masses since Epstein and Mayeda (1953) introduced the method to oceanography. The ratio is generally expressed as $\delta^{18}O$, which represents the deviation of the sample from an international standard such as Vienna-Standard Mean Ocean Water (V-SMOW), that is,

$$\delta^{18}O(‰) = 1000(^{18}O/^{16}O_{\text{sample}} - {}^{18}O/^{16}O_{\text{V-SMOW}}) \div (^{18}O/^{16}O_{\text{V-SMOW}}). \quad (1)$$

Cooper et al. (1997) describe details of the analysis methods, which have standard errors of about 0.1‰ in $\delta^{18}O$. Strain and Tan (1993) discuss how melting and freezing affects the distribution of $\delta^{18}O$ as a function of depth and salinity.

3. Hydrography

During our surveys and drifter deployments in 1995, the coastal waters off Siberia were ice free (Fig. 3). The waters of the East Siberian Sea are both fresh and cold (Figs. 5 and 6). Surface temperatures vary between 0° and 2°C while bottom temperatures are near the freezing point. At depth we find large horizontal salinity gradients but almost no temperature gradients. This contrasts in all respects with the hydrography in the adjacent Chukchi Sea, which receives Pacific waters from the Bering Sea through Bering Strait (Coachman et al. 1975). In the Chukchi Sea surface and bottom waters reach 7°C and 2.5°C, respectively. In contrast to the East Siberian Sea, temperature gradients in the Chukchi Sea are large while salinity gradients are small. The transition occurs at Long Strait near the date line where we find both the coldest (<0°C) and most saline (>32.5 psu) waters. These are remnant waters from the previous winter (Coachman et al. 1975) and were probably formed within the polynya that frequently forms along the south coast of Wrangel Island (Cavalieri and Martin 1994).

On both shelves inshore waters are generally colder, saltier, and thus denser than offshore waters. This trend is particularly clear in Fig. 7, which shows salinity and $\delta^{18}O$ distributions on sections K, A, B, and C (see Fig. 5 for locations). Section K extends alongshore from the Kolyma plume toward Ayon Island while sections A, B, and C extend across the shelf. We deployed drifters along sections A, B, and C. Frontal features are not resolved well by the 20-km station spacing of the sur-

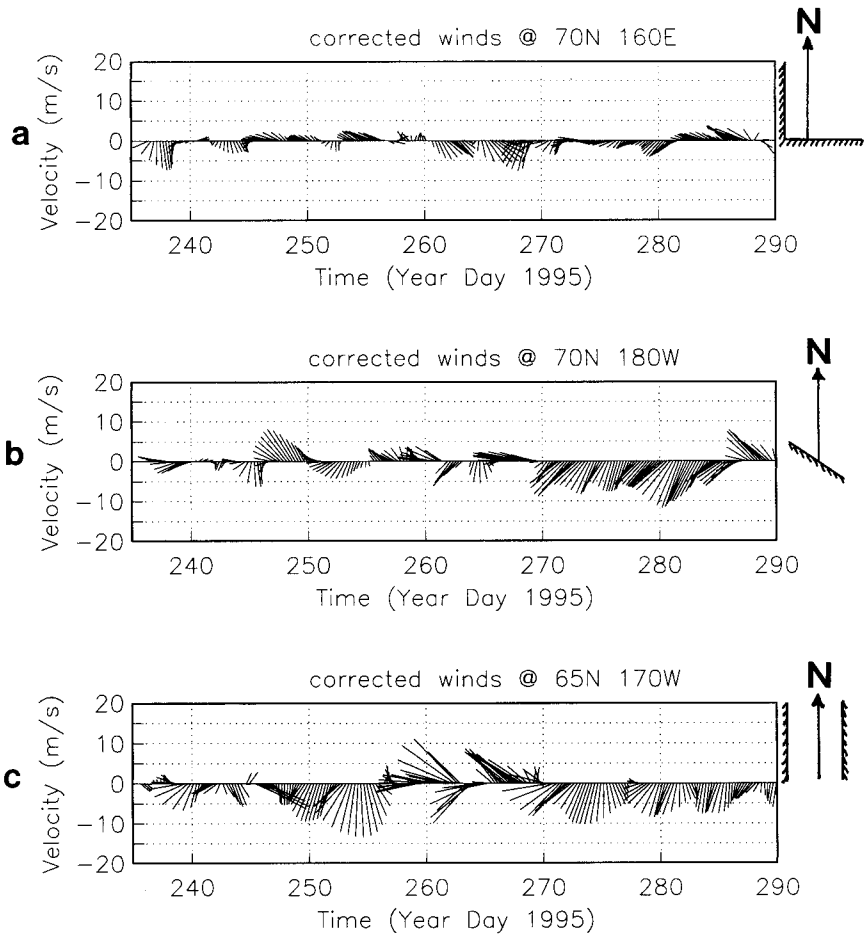

FIG. 4. Time series of wind vectors near (a) the Kolyma Delta, (b) Long Strait, and (c) Bering Strait. Note the increasing winds from west to east. The orientation of the coastline and true North is indicated to the right of each panel.

vey; however, large horizontal salinity (and thus density) gradients occur throughout the study area. The ice edge is present on sections B and C about 160 km and 110 km from the coast, respectively (Fig. 7). Property gradients are most pronounced in Long Strait (section C) as compared with the more westward sections B and A. Low $\delta^{18}O$ values indicate that the river plume extends far offshore in dilute form. We find fresh ($S < 28$ psu) and isotopically light ($\delta^{18}O > -4‰$) waters both about 100 km to the north of Ayon Island on section A (Fig. 7b) and 100 km to the west of Ayon Island on section K (Fig. 7a). Inshore salinities increase from the Kolyma River (section K) eastward toward Long Strait (section C). These reach values of about 30, 32, and 33 psu along sections A, B, and C, respectively (Fig. 7); however, along section K we find Kolyma plume waters inshore where salinity and $\delta^{18}O$ drop below 19 psu and -9.0%. The waters thus become progressively fresher and isotopically lighter toward the Kolyma Delta along section K and offshore along section A.

The property distributions of section B warrant additional comment since they foreshadow the main result of this study: a mean westward flow due to baroclinic forcing from a retreating ice edge. The temperature patterns are decoupled from density patterns and reflect solar heating of the surface waters (Fig. 8). The freshest waters are offshore at the location of the ice edge; however, we also find a shallow wedge of warm and somewhat fresher surface water about 30 km from the coast. A 30-m thick pool of cold and salty waters overlies a bathymetric depression 40 km wide about 50 km from the coast. Dense bottom waters are advected preferentially over this depression from polynyas around Wrangel Island. Drifters deployed at the three inshore stations of section B indicate a cyclonic surface circulation over this topographic depression. Isopycnals offshore of this depression contact both the surface and the bottom. Figure 9a shows the thermal wind shear relative to no flow at the bottom; however, it indicates a baroclinic westward surface circulation of about 0.05 m s^{-1}. Figure 9b compares this estimate with alongshore velocities derived from drifters that pass section B. While the agree-

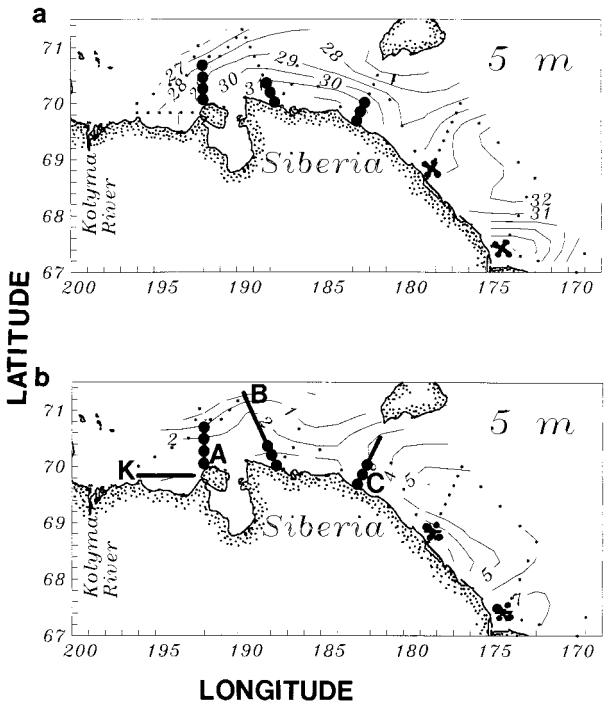

FIG. 5. Maps of (a) salinity and (b) temperature at 5-m depth in the East Siberian and Chukchi shelf seas. Drifter deployment locations are shown as large circles; CTD cast locations are shown with a small asterix. The survey was conducted from 24 Aug through 1 Sep 1995.

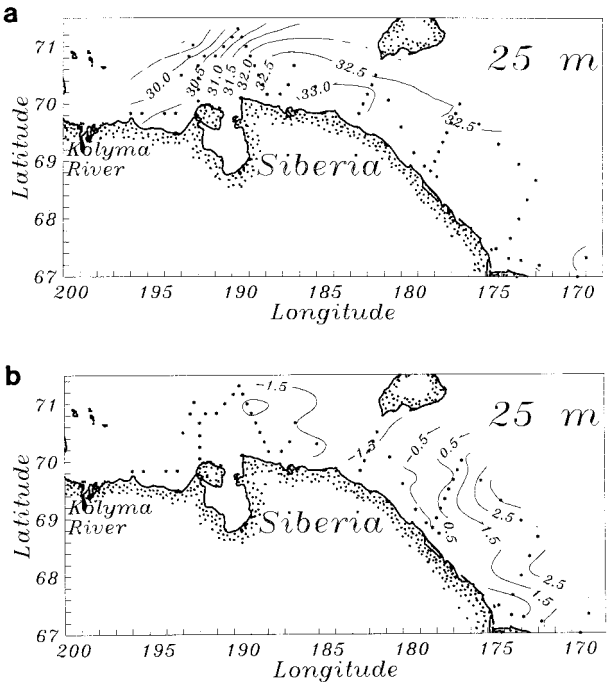

FIG. 6. As in Fig. 5 but 25 m below the surface.

ment is not perfect, the drifter-derived velocities show, in the mean, the same trend as the thermal wind, that is a 0.05 m s^{-1} westward surface flow. We discuss more details of the observed velocity fields in section 5.

4. Water masses

In this study we consider three water masses. These are resident shelf waters, freshwater from river discharges, and freshwater from seasonal ice melt. Östlund and Hut (1984), Cooper et al. (1997), Grebmeier et al. (1990), Schlosser et al. (1994), and Macdonald et al. (1995) all use salinity and $\delta^{18}O$ measurements to distinguish between river discharge and ice melt. In order to properly do so, however, one needs to prescribe numerical values for the end members that potentially contribute to the admixture. While it is straightforward to find values for the riverine input that we discuss next, it is more problematic to find an adequate $\delta^{18}O$ value for the ice melt end member.

Östlund and Hut (1984) suggest a value of -21.0 ± 0.7‰ for riverine waters that enter the Arctic Ocean; Grebmeier et al. (1990) consider a value of -22.0 ± 0.3‰ appropriate for the Yukon River, Alaska; and Macdonald et al. (1995) use a value of -20.3‰ and -18.3‰ for the Mackenzie River, Canada, in the summer and winter, respectively. Létolle et al. (1993) cite river values for the Eurasian Arctic that decrease west to east from -12.7‰ for fjords in northern Norway to -23.8‰ for the Indigirka River. It is more difficult and ambiguous to assign a $\delta^{18}O$ value for ice melt. Macdonald et al. (1995) distinguish between river and sea ice because the $\delta^{18}O$ of their ice samples varies from -16.0‰ to -2.0‰. Ideally, we need a third tracer (e.g., barium; Guay and Falkner 1998) to separate sea ice melt from river ice melt. Such samples are not available for this study.

In our study area $\delta^{18}O$ values vary from the isotopically heavy value of -1.00‰ to the isotopically light value of -9.57‰. The $\delta^{18}O$ versus S scatter of East Siberian Sea waters indicates a regression $\delta^{18}O = -17.9 + 0.52S$ that explains 76% of the variance of 33 surface samples. Table 1 lists this regressions along with 95% confidence levels for the estimated parameters. Fofonoff and Bryden (1975) thoroughly discuss such error statistics. Our regression for the East Siberian Sea is significantly different from the regression for the western Chukchi Sea where we find $\delta^{18}O = -8.6 + 0.24S$. This regression explains 67% of the variance of 40 surface samples. The Chukchi Sea surface waters are isotopically heavier than the East Siberian Sea waters and resemble Anadyr waters (Cooper et al. 1997; Grebmeier et al. 1990). The lack of silica (not shown), however, indicates that the Chukchi waters are not derived from this source but instead must represent sea ice melt. Furthermore, Grebmeier et al. (1990) find a $\delta^{18}O$ versus S regression for the eastern Chukchi and northern Bering seas ($\delta^{18}O = -24.9 + 0.71S$) that drastically contrast with our regression for the western Chukchi. Riverine discharges such as the Yukon River into the Bering Sea

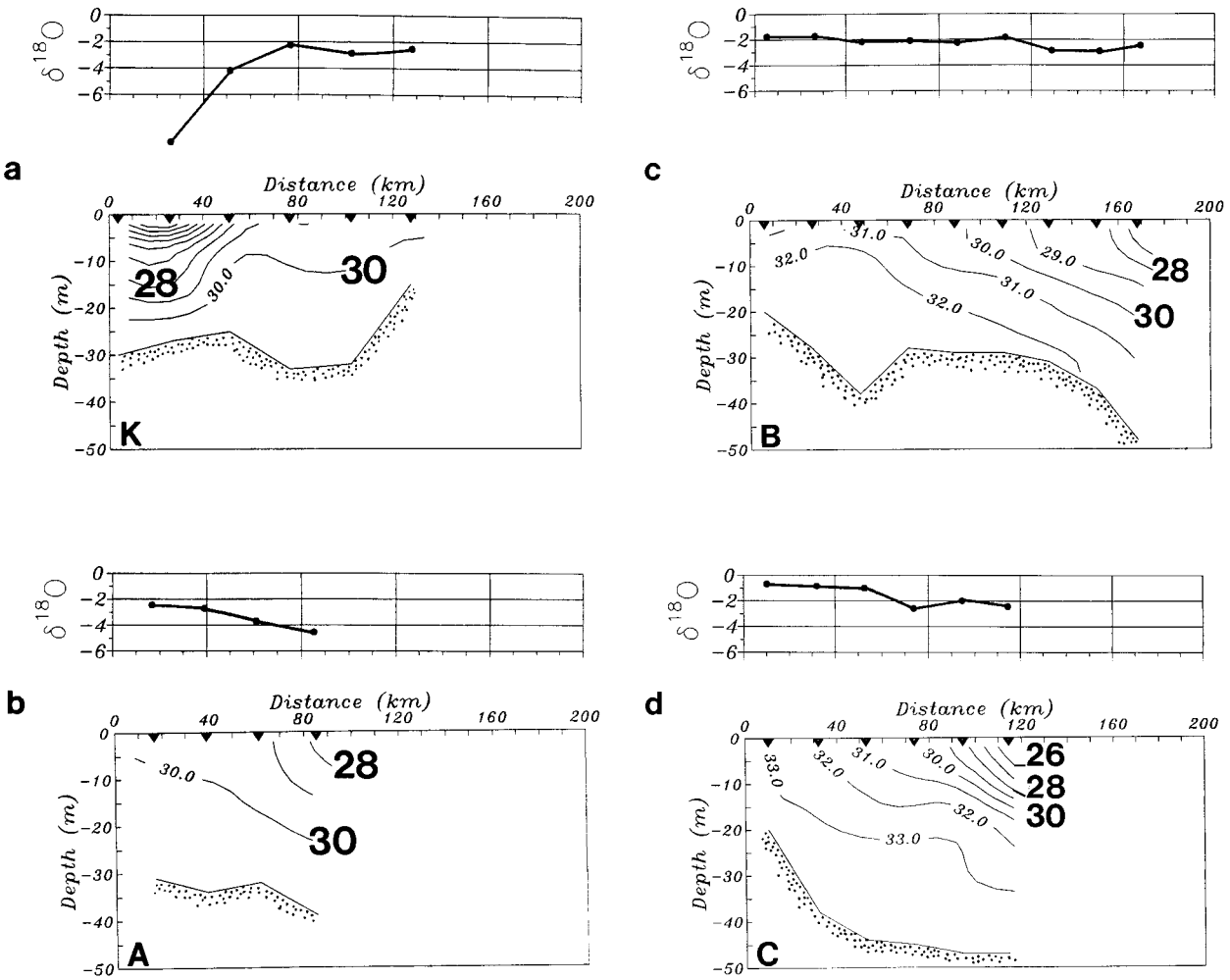

FIG. 7. Salinity transect and $\delta^{18}O$ profiles at surface for (a) section K along the shelf from the Kolyma plume toward Ayon Island, the view is toward north; (b) section A across the shelf off Ayon Island, the view is toward west; (c) section B across the shelf near 190°W, the view is toward west; and (d) section C across Long Strait, the view is toward west. The locations are highlighted in Fig. 5.

contribute to the buoyancy-driven coastal current along the Alaska coast of the eastern Chukchi Sea (Paquette and Bourke 1974), which leaves the shelf through Barrow Canyon (Münchow and Carmack 1997). This finding becomes significant for the East Siberian Sea because closer inspection of the $\delta^{18}O$ versus S scatter suggests two distinct linear regression (Fig. 10). Sorting the data subjectively, we find one regression labeled ''ice-melt waters'' in Fig. 10a,

$$\delta^{18}O = -8.3 + 0.22S, \quad (2)$$

that resembles the western Chukchi Sea regression. It explains 84% of the variance of 18 samples. A second regression labeled ''riverine waters'' in Fig. 10b,

$$\delta^{18}O = -19.5 + 0.56S, \quad (3)$$

is most consistent with the Kolyma River discharge as a source of freshwater. It explains 93% of the variance for 37 samples. The uncertainties in the estimated parameters $\delta^{18}O(S = 0)$ and $d(\delta^{18}O)/d(S)$ at the 95% level of confidence are less than 1.6‰ and 0.06, respectively. We note, however, that neither the end-member $\delta^{18}O(S = 0) = -8.3 \pm 1.38$‰ nor the end-member $\delta^{18}O(S = 0) = -19.5 \pm 1.55$‰ represent pure sea ice melt or pure Kolyma River water. Pure sea ice melt has $\delta^{18}O \approx 0$‰ after isotopic fractionation during freezing and a salinity of about 6 psu (Macdonald et al. 1995). The Kolyma River has $\delta^{18}O \approx -22.4$‰ (Vaïkmae 1990; cited by Létolle et al. 1993).

We interpret the two regression curves of Fig. 10 to represent (a) mixing of salty ambient polar shelf water with isotopically light Kolyma River plume waters and (b) mixing of salty ambient polar shelf water with isotopically heavy ice melt that contains a fraction of river ice melt. Surface samples from the western Chukchi Sea have $\delta^{18}O$ versus S regressions very similar to the ice melt samples of the adjacent East Siberian Sea (Table 1). This observation could indicate similar sources and

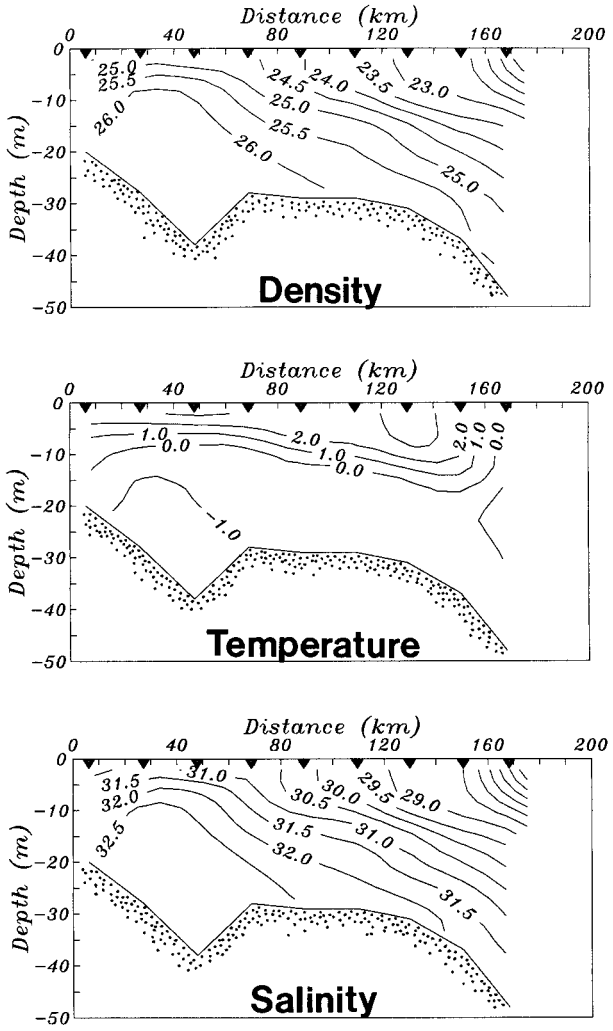

FIG. 8. Density, temperature, and salinity across section B.

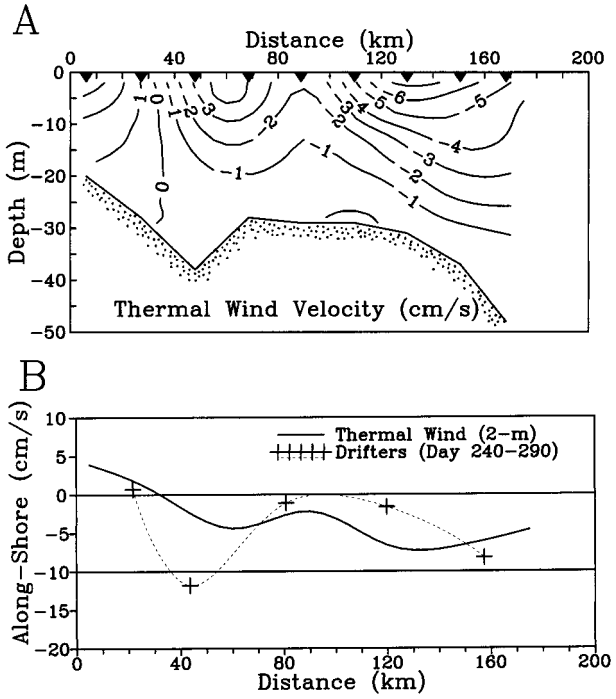

FIG. 9. Thermal wind velocities relative to no flow at the bottom: (a) The alongshelf thermal wind velocity for the entire section B. (b) Comparison of the thermal wind velocity at 2-m depth (solid line) with alongshelf velocities estimated from drifters that pass section B (dashed line with "+").

freezing/melting histories (Strain and Tan 1993). Nevertheless, we here distinguish three water masses. These are ice melt ($\delta^{18}O = -0‰$, $S = 6$ psu), ambient polar shelf ($\delta^{18}O = -1.0‰$, $S = 33$ psu), and, finally, river waters ($\delta^{18}O = -22.4‰$, $S = 0$ psu). Assuming a three-point admixture as well as the conservation of mass, salt, and $\delta^{18}O$ (Macdonald et al. 1995), we find that East Siberian shelf waters at any location contain less than 16% ice melt, frequently contain more than 10% river waters, and always contain more than 54% polar shelf waters. Uncertainties in these percentages due to uncertainties in the assigned salinity and $\delta^{18}O$ for the source waters are about 2%–3%.

The spatial distribution of the three water masses reveals two distinct source regions of freshwater. Figure 11a indicates the fraction of riverine waters resident in

TABLE 1. Regression coefficients between $\delta^{18}O$ and salinity S, i.e., $\delta^{18}O = a + bS$ along with 95% confidence limits Δa and Δb.

Group of samples	$a \pm \Delta a$(‰)	$b \pm \Delta b$(−)	r^2	N
All East Siberian Sea, ice melt	−8.3 ± 1.38	0.22 ± 0.047	0.84	18
All East Siberian Sea, river water	−19.5 ± 1.55	0.56 ± 0.053	0.93	37
Surface East Siberian Sea, river water	−19.8 ± 1.84	0.58 ± 0.065	0.94	20
Surface East Siberian Sea, ice melt	−8.4 ± 2.06	0.22 ± 0.072	0.76	13
Surface East Siberian Sea	−17.9 ± 2.93	0.52 ± 0.103	0.76	33
Surface Chukchi Sea	−8.6 ± 1.59	0.24 ± 0.054	0.67	40
Bottom Chukchi/Bering Sea (Grebmeier et al. 1990)	−24.9	0.71	0.78	60
Bottom Chukchi shelf (Cooper et al. 1997)	−17.3	0.50	0.69	264
Surface Laptev Sea (Létolle et al. 1993)	−18.9	0.79	1.00	15

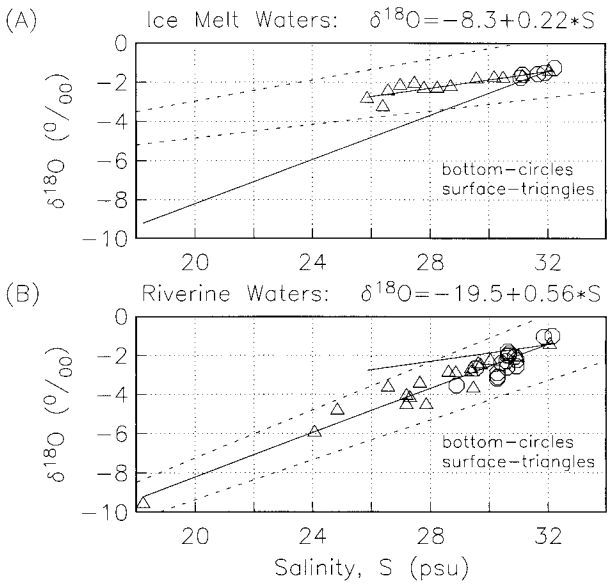

FIG. 10. Oxygen isotope ratios (δ^{18}O) as a function of salinity (S) from water samples collected in the East Siberian Sea. The data are sorted for (a) ice melt waters and (b) meteoric waters. Both linear regression curves for (a) and (b) are shown on both plots. Triangles and circles indicate near-surface and bottom samples, respectively. The dashed lines represent the upper and lower limit of the 95% confidence levels for the regressions.

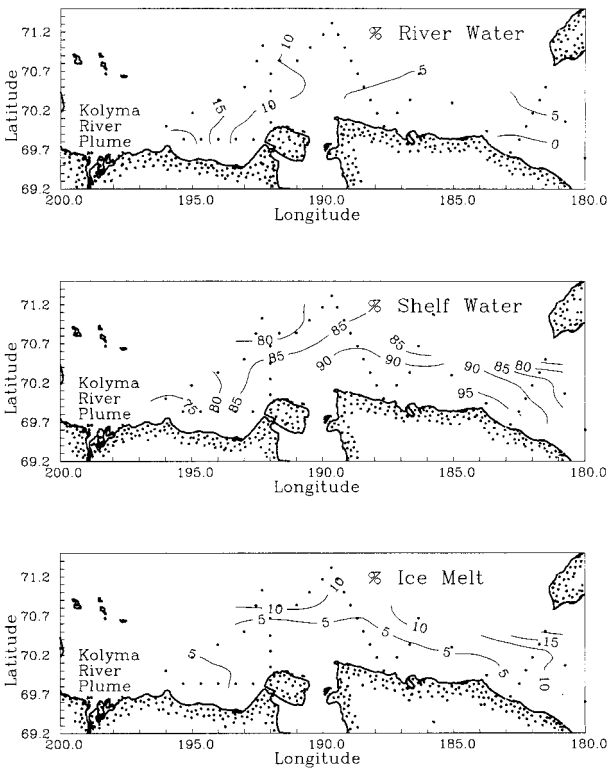

FIG. 11. Maps of water mass distribution in surface waters of the East Siberian Sea based on measurements of salinity and δ^{18}O along with mass conservation of volume, salt, and δ^{18}O.

the surface waters of the eastern East Siberian Sea. Near the Kolyma River delta almost 20% of the water contains riverine freshwater; however, this fraction declines rapidly to less than 10% within about 100 km both to the north and east. The maximum of the ice melt fraction is found near the date line off Wrangel Island (Fig. 11b) where 20% of the surface waters consist of recent ice melt. Wrangel Island is also the location where the permanent polar ice pack always extends farthest south (Fig. 3) and, in some years, never disappears. In contrast, the nearshore waters along the coast off Siberia contain less than 5% of ice melt but more than 90% of ambient shelf waters. These are the cold, salty, and isotopically heavy waters that we find both at depth and in the western Chukchi Sea; however, we here also find them at the surface to the east of Ayon Island. They represent remnant winter waters.

5. Kinematics

a. Initial displacement

During the summer of 1995 we released 39 surface drifters into ice-free waters of the East Siberian Sea (7 drifters), the Chukchi Sea (26 drifters), and Long Strait (6 drifters). At the end of the ice-free summer season, 19 drifters were floating in the East Siberian Sea and 5 in the Chukchi Sea. The net surface drift thus was westward. (An additional 10 drifters stranded or entered coastal lagoons in the East Siberian and Chukchi Seas; 5 drifters failed during the first 2 months after their deployment.)

The westward drift contradicts both prior measurements and dynamical expectations. For example, Sverdrup (1929) reports that the shelf flow in the East Siberian Sea is eastward toward Long Strait and is driven by lateral density gradients induced by buoyant river discharges. Specifically, he writes that

> . . . great quantities of drift wood are found along the coast of the Kolima River toward the east, and this drift wood must originate from the Kolima River or rivers still further west, indicating that it has been carried by currents to the east. The question arises whether this east-going current, carrying light water with low salinity, enters the Chukotsk Sea or not. . . . We know that drift wood becomes very scarce at the coast when it bends south-east in longitude 170E, and this circumstance indicates that the coastal current turns toward the north in this region. Furthermore, none of our observations east of Wrangell Island has given low salinities.
>
> (Sverdrup 1929, p. 74).

The oceanographic atlas of the U.S. Weather Bureau for the Arctic Ocean published by the direction of the Chief of Naval Operations (U.S. Weather Bureau 1957) depicts a uniform 0.15–0.50 m s^{-1} strong eastward surface flow from the East Siberian Sea through Long Strait

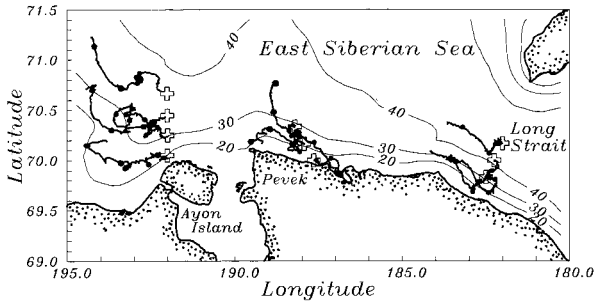

FIG. 12. Trajectories of surface drifters deployed along the three salinity sections shown in Fig. 7. Circles on the trajectories are 2 days apart.

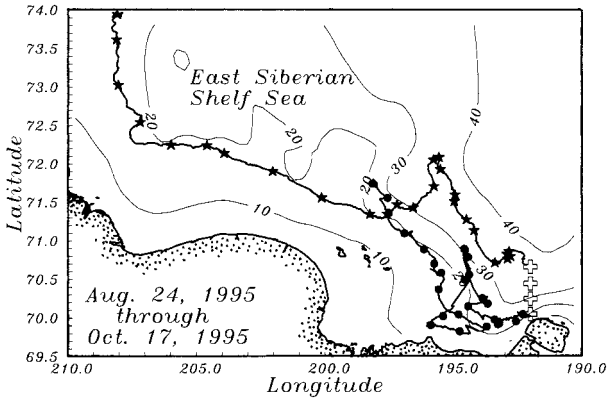

FIG. 13. Trajectories of an inshore and offshore drifter closest to the Kolyma River. Note the rapid westward movement of the offshore drifter, which we speculate is trapped in a frontal zone.

toward Alaska. Coachman and Rankin (1968) comment on the highly variable subtidal circulation and speculate that the currents respond to local winds and pressure gradients.

Figure 12 shows the drifter trajectories for 2 weeks after their deployment along sections A, B, and C. The drifters were deployed in a 2-day period within 80 km from the coast and 30 km from the ice edge. All drifters moved northwestward in a spatially and temporally coherent fashion at the largest spatial scale of about 300 km. At smaller spatial scales, however, we find differences in the initial trajectories. For example, on section A we deployed 4 drifters along a line that extended offshore into a pool of Kolyma River plume waters fresher than 28 psu. The drifter deployed farthest offshore into these waters exhibits a most spectacular trajectory. It first stalls for almost 8 days before it moves northward and rapidly separates from all other drifters (Fig. 13). Its Lagrangian velocity fluctuations correlate only weakly with the winds; that is, we believe that this drifter accurately tracks the water with its drogue intact. It appears that this drifter was captured within a frontal region. In contrast, the 3 inshore drifters move slowly westward while looping both cyclonically and anticyclonically at wind-dominated timescales of 3–8 days. On section B the inshore drifter moves rapidly southeastward while the central and offshore drifter move slowly in the opposite direction (Fig. 12). This cyclonic circulation with westward flow offshore is consistent with the thermal wind relation with no flow at depth (Fig. 9). In contrast, the drifters of section C move almost in unison first onshore then rapidly toward the west. The overall direction of all these surface displacements is consistent with the internal pressure field of an offshore source of buoyancy such as the melting and retreating ice edge (Fig. 9).

b. Temporal and spatial perspectives

Figure 14 shows current vectors on a map of the bottom topography of the East Siberian Sea along with the trajectories from which the velocity vectors were estimated. The current vectors constitute the surface circulation during the ice-free summer season. Instantaneous subtidal velocities reach 0.5 m s^{-1} and indicate a generally northwesterly flow. Flow reversals occur frequently in both space and time. Most vectors align themselves along isobaths. This includes the shallow Kolyma Canyon to the west of Ayon Island where we discern an anticyclonic circulation around the canyon rim. We next discuss spatial and temporal views of the data.

An example of the spatial variability of the flow field is shown in Fig. 15 as a 3-day sequence of velocity snapshots. Instantaneous velocity vectors from 18 drifters depict synoptic currents together with the ice edge. On 12 September (day 255) the ice edge is about 150 km from the coast in the East Siberian Sea. Winds are less than 5 m s^{-1} and change direction from southerly to northerly (Fig. 4). The flow, however, exceeds 0.2 m

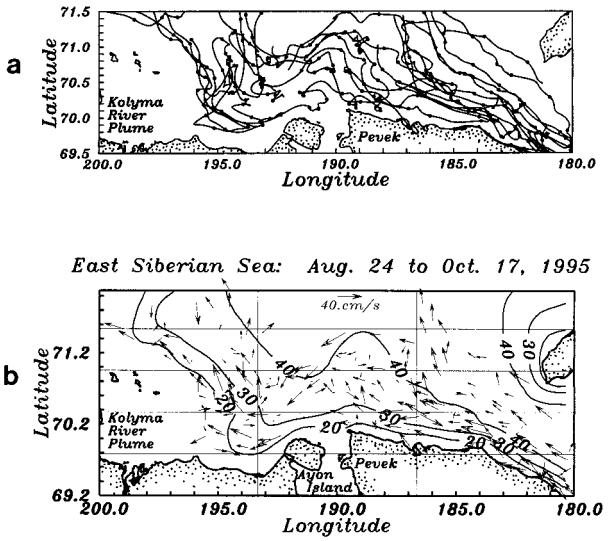

FIG. 14. Map of (a) drifter trajectories and (b) current vectors. The grid in (b) indicates spatial bins used to estimated averaged properties. The bottom topography is shown also.

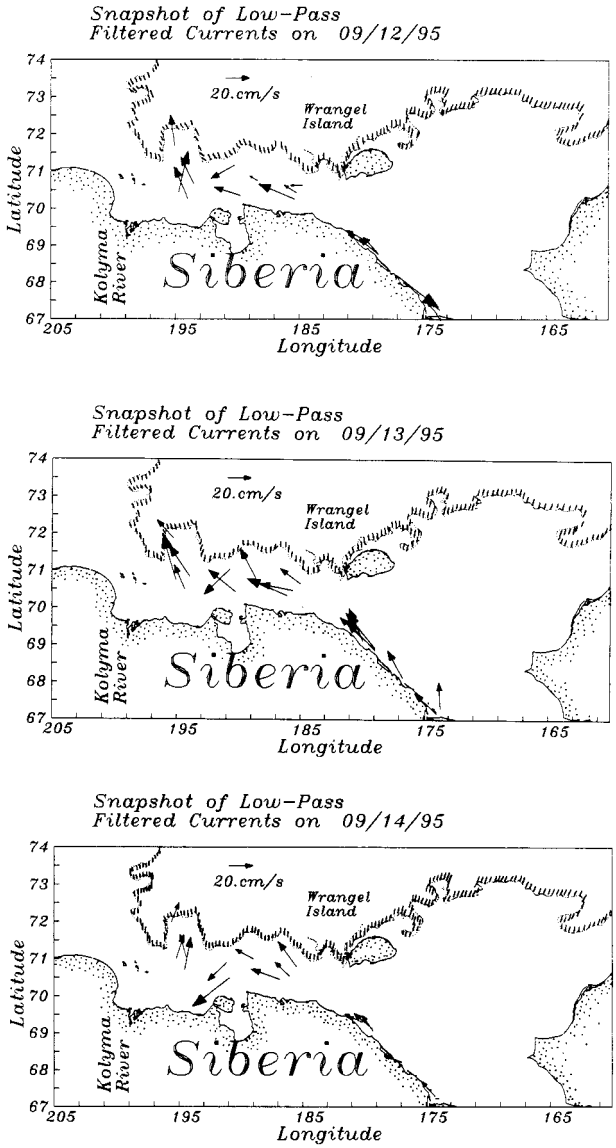

FIG. 15. Sequence of velocity snapshots in the East Siberian and Chukchi shelf seas 12, 13, and 14 Sep. Note the spatial coherence as well as the northward flow near a large opening in the ice edge.

s^{-1} in a generally northwestward direction in both the Chukchi and the East Siberian Seas. The flow does not appear to be forced by the weak winds. Furthermore, the flow is surprisingly coherent at spatial scales from 100 km to 1000 km. We also note a large 100 × 100 km^2 opening in the ice at about 195°W long. The location of this ''bay'' corresponds to the location of a 0.3 m s^{-1} northward flow. This northward flow had persisted for about 10 days prior (not shown). We suspect that the opening ''bay'' is created by the advection of warmer surface waters from the south.

We depict the temporal variability of the surface flow in the East Siberian Sea in Fig. 16 along with a time series of wind stress vectors. The two time series of drifter-derived velocities represent a spatial average for an offshore and an inshore location. More specifically, we averaged the velocities of all drifters from a spatial bin 810 × 130 km^2 at a given time (see Fig. 14 for the location of the spatial bins). Between 2 and 15 drifters contribute to the average velocity. The time series show that spatial mean flows frequently exceed 0.2 m s^{-1} and are generally to the northwest. A reversal occurs between yearday 260 and 270. It is not apparent that this event correlates strongly with the local wind stress; a similar stress three times as large on day 282, for example, does not cause a reversal. A formal correlation of the wind stress and velocity vectors confirms this weak wind forcing. Maximum complex vector correlation between currents and winds occur with a lag of about 6 h at an angle 93° (100°) to the left of the wind for an inshore (offshore) spatial bin. The veering angle to the left of the wind is surprising; however, the vector correlation is only 0.4 (0.3) inshore (offshore) and thus not significantly different from zero (Bartlett 1978). Only about 16% (inshore) and 9% (offshore) of the current variance is explained by the variance of the wind. We thus conclude that forces other than the surface wind stress contribute to the dynamics of the spatially averaged velocity fields in the East Siberian Sea. Since the thermal wind relation can explain the observed mean flow in the alongshelf direction (Fig. 9), baroclinic forcing contributes to the dynamics. The lateral buoyancy fluxes of a melting and retreating ice edge constitutes such forcing.

c. Lagrangian scales

Lagrangian statistics $\langle \cdot \rangle_L$ result from ensemble-averaging properties of drifters that were deployed in an area of interest. We deployed 10 drifters in an area about 400 × 70 km^2 (Fig. 12) within about 2 days. Their individual mean velocities vary between 0.05 and 0.12 m s^{-1} during the 50 days that they drifted freely in the East Siberian Sea. Their mean directions vary between 133° and 164° counterclockwise from true East. The strong directionality of the flow to the northwest contrasts with all known velocity observations from this shelf (Sverdrup 1929; Coachman and Rankin 1968; and U.S. Weather Bureau 1957).

Decomposing the Lagrangian velocities into a mean and fluctuating part for the eastward (u) and northward (v) velocity components, that is,

$$u(t) = \langle u \rangle_L + u'(t) \qquad v(t) = \langle v \rangle_L + v'(t),$$

we find that the overall mean velocity ($\langle u \rangle_L$, $\langle v \rangle_L$) is (−0.066, 0.042) m s^{-1}. The variances about this mean velocity are $\langle u'u' \rangle_L = 0.0218$ m^2 s^{-2}, $\langle v'v' \rangle_L = 0.0210$ m^2 s^{-2}, and $\langle u'v' \rangle_L = 0.0004$ m^2 s^{-2} (Table 2). The autocovariances $\langle u'u' \rangle_L$ and $\langle v'v' \rangle_L$ represent rms speeds of about 0.15 m s^{-1}. The fluctuating motions are thus about twice as strong as the mean motions. Additionally, they are spatially homogeneous at the largest scale and

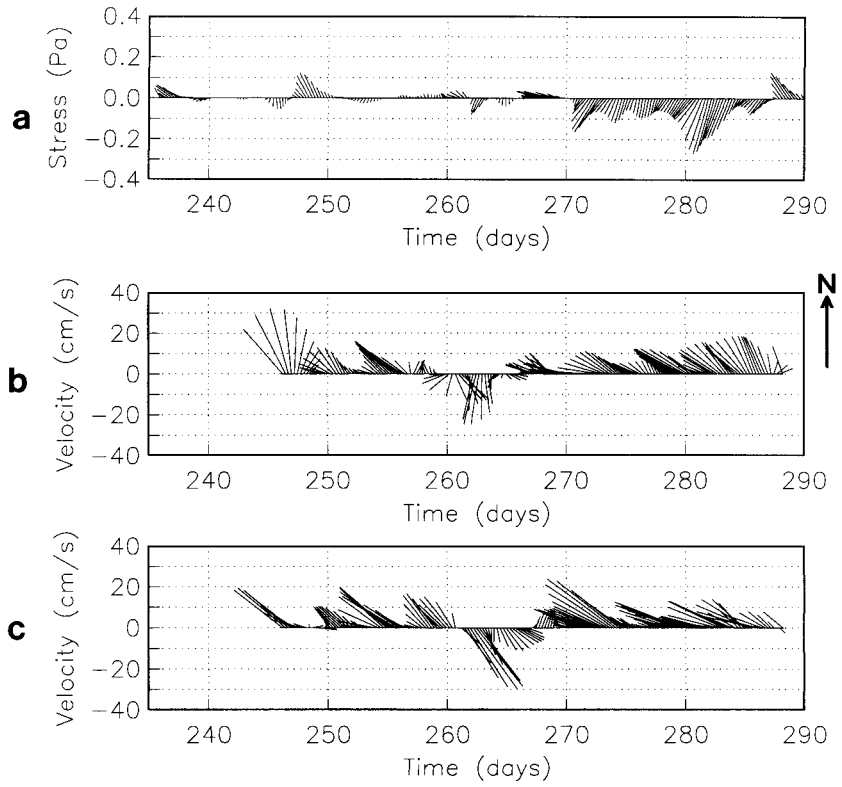

FIG. 16. Time series of (a) wind stress and [(b) and (c)] spatially averaged drifter velocities in the East Siberian Sea for (b) inshore and (c) offshore. Note the temporal and spatial coherence of the average flow fields with velocity vectors generally toward the northwest. Note also the very weak correlation of the flow with the winds.

we can, if we assume stationarity of the velocity field, apply the theory of Taylor (1921) to study dispersion on this shelf. We will do so below after we discuss temporal and spatial scales of variability.

Assuming that velocity is a Gaussian variable, we find that the statistical uncertainty of the overall mean is $\delta = 1.96(\langle u'u'\rangle_L T_L/T)^{1/2} \approx 0.028$ m s^{-1} at the 95% level of confidence. The ratio T/T_L estimates the statistical degrees of freedom for a record length T and a Lagrangian autocorrelation scale T_L. Following Poulain and Niiler (1989), we define T_L as the integral of the normalized versions of the Lagrangian autocorrelation functions $R_{uu}(\tau)/R_{uu}(\tau = 0)$ and $R_{vv}(\tau)/R_{vv}(\tau = 0)$ to the first zero crossing; τ represents the lag time. The functions $R_{uu}(\tau)$ and $R_{vv}(\tau)$ are defined as

$$R_{uu}(\tau) = \langle u'(t)u'(t + \tau)\rangle_L$$

$$R_{vv}(\tau) = \langle v'(t)v'(t + \tau)\rangle_L.$$

Integrating the normalized autocorrelation functions to their first zero crossing at 4 and 5.5 days (Fig. 17), we find that meridional and zonal integral timescales have first maxima near 3.5 and 2.5 days, respectively. This constitutes an upper limit of T_L. The timescales relate to an integral space scale L_L through

$$L_L = (\langle u'u'\rangle_L)^{1/2} T_L,$$

which in the East Siberian Sea is about 43 and 35 km in the meridional and zonal direction, respectively. Decorrelation time and space scales thus are about 3 days and 40 km. We use these scales to estimate degrees of freedom within our dataset.

The integral of $R_{uu}(\tau)$ and $R_{vv}(\tau)$ with respect to τ represents a single particle diffusivity if the flow is both homogeneous and stationary (Poulain and Niiler 1989).

TABLE 2. Global statistics and scales.

	Eulerian	Lagrangian
$\langle u\rangle$ (m s^{-1})	−0.092 ± 0.021	−0.066 ± 0.028
$\langle v\rangle$ (m s^{-1})	0.049 ± 0.019	0.042 ± 0.027
$V(u)$ (m s^{-1})^2	0.0236	0.0218
$V(v)$ (m s^{-1})^2	0.0191	0.0210
$V(uv)$ (m s^{-1})^2	−0.0046	0.0004
$T^{(x)}$ (h)	n/a	65
$T^{(y)}$ (h)	n/a	84
$L^{(x)}$ (km)	n/a	43
$L^{(y)}$ (km)	n/a	34
K_{xx} (10^3 m^2 s^{-1})	n/a	3.5
K_{yy} (10^3 m^2 s^{-1})	n/a	2.5

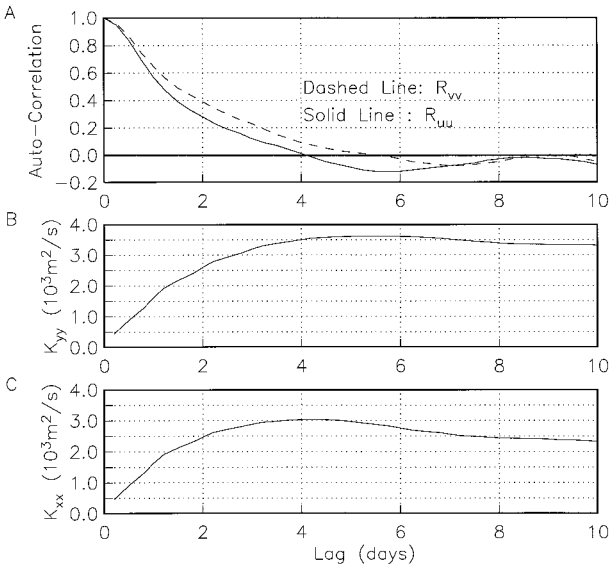

FIG. 17. Normalized Lagrangian autocorrelation functions (a) and derived diffusivities K_{xx} (b) and K_{yy} (c). The integral timescales are about 3 days while diffusivities reach 3–4 ($\times 10^3$ m^2 s^{-1}).

Figures 17b and 17c depict the diffusivities K_{xx} and K_{yy} as a function of lag time, respectively. Using Taylor's (1921) theory of diffusion to interpret our data, we distinguish between initial dispersion for times $\tau \ll T_L$ where the diffusivity varies linearly with lag time τ and a random walk regime for times $\tau \gg T_L$. The initial dispersion lasts for about a day while for lag times longer than 8 days the diffusivities reach values of about 3.5×10^3 and 2.5×10^3 m^2 s^{-1} for the zonal and meridional component, respectively. These values are large, especially in the across-shelf (meridional) direction and resemble those of midlatitude open ocean studies. For example, Poulain and Niiler (1989) report diffusivities of about 3–4 ($\times 10^3$ m^2 s^{-1}) for the California Current System, Krauss and Böning (1987) find diffusivities in the range of 2–8 ($\times 10^3$ m^2 s^{-1}) for the North Atlantic, and Middleton and Garrett (1986) use icebergs off Labrador to estimate an isotropic diffusivity of about 1.1×10^3 m^2 s^{-1}. In contrast, Davis (1985) finds 3.1×10^3 and 0.08×10^3 m^2 s^{-1} for an alongshelf and across-shelf diffusivity within about 10 km off California. Münchow and Garvine (1993) report diffusivities of about 2×10^3 and 0.5×10^3 m^2 s^{-1} for the Delaware coast in the along- and across-shelf directions, respectively. The dispersive characteristics of drifters deployed in the strongly stratified East Siberian shelf sea thus resemble open-ocean drifters at midlatitudes more than they resemble drifters released into the coastal ocean.

d. Eulerian currents

Eulerian statistics $\langle \cdot \rangle_E$ result from averaging properties of drifters that are found in an area of interest. The overall Eulerian mean velocities ($\langle u \rangle_E$, $\langle v \rangle_E$) are (-0.092, 0.049) m s^{-1} and agree with the Lagrangian global mean to within the 95% confidence limits (Table 2). Variances about the Eulerian mean velocities are similar also; that is, $\langle u'u' \rangle_E = 0.0236$ m^2 s^{-2}, $\langle v'v' \rangle_E = 0.0191$ m^2 s^{-2}, and $\langle u'v' \rangle_E = -0.0046$ m^2 s^{-2}. These estimates represent a single average over a box that spans an area of about 810×260 km^2 (see Fig. 12 for locations). In order to increase the spatial resolution we next bin average velocity data into boxes that extend 270 km and 65 km in the zonal and meridional directions, respectively. Figure 14 shows these boxes as a grid along with 204 statistically independent velocity observations. The grid size constitutes a compromise between spatial resolution and statistical reliability. We treat speed and direction as independent variables assuming that speed follows a Gaussian normal distribution while directions follow the von Mises distribution (Mardia 1972). To achieve reliable results, we require each bin-averaged velocity estimate to have at least 5 degrees of freedom (15 drifter days), to contain information from at least 5 different drifters, and to have a preferred direction; that is, an estimate must pass the Raleigh test at the 95% confidence level (Mardia 1972). Table 3 lists nine significant time-mean velocity estimates as well as two insignificant estimates along with their uncertainties. The error bars contain the array bias $\Delta \mathbf{u} = \kappa(\nabla N)/N$ (Davis 1991); here κ is the 2×2 diffusivity tensor with K_{xx} and K_{yy} its diagonal elements, ∇N is the spatial gradient of drifter numbers, and N is the number of drifters within a box.

Figure 18 shows the Eulerian mean flow of the East Siberian Sea. The surface flow generally follows isobaths, which in the western portion of our study area bend northward. At that location the surface flow turns northward also. It diminishes in magnitude from almost 0.2 m s^{-1} near Long Strait in the east to less than 0.05 m s^{-1} near the Kolyma Delta in the west. The westward flow increases from inshore to offshore. This offshore intensification of the flow correlates with the density field in the thermal wind sense. The 100-km-wide region of enhanced lateral density gradients is due to a retreating ice edge that forces the mean flow.

The principal axes of variations represent the deviations from the mean currents. These axes are the square root of the eigenvalues of the Reynolds stress or covariance tensor (Kundu and Allen 1976). Figure 19 depicts these axes for each spatial bin; a circle with the radius of the semimajor axes surrounds each estimate in order to emphasize the ellipticity of the time-varying Eulerian currents. Semimajor axes are generally aligned with the bottom topography, which indicates that barotropic dynamics dominate the fluctuating motions. This finding agrees with Weingartner et al. (1998) based on current meter mooring data from the Chukchi Sea. However, flows are strongly polarized near the coast, become more circular offshore, and correlate only weakly with the local winds. A substantial fraction of the observed

TABLE 3. Eulerian mean currents and 95% confidence levels.

	Longitude (west)	Latitude (north)	Degrees of freedom	Drifters	Speed (m s^{-1})	Direction (ccw from east)
1*	194.7	70.1	15	4	0.05 ± 0.085	130 ± 180
2*	195.0	70.7	16	5	0.07 ± 0.077	124 ± 68
3	196.2	71.2	14	6	0.10 ± 0.077	127 ± 50
4	197.3	71.8	9	6	0.11 ± 0.101	129 ± 55
5	189.9	70.2	27	10	0.08 ± 0.054	174 ± 50
6	190.3	70.7	40	14	0.08 ± 0.043	151 ± 40
7	189.9	71.2	21	9	0.10 ± 0.047	151 ± 37
8	180.8	69.5	37	14	0.09 ± 0.070	146 ± 38
9	183.4	70.1	34	11	0.14 ± 0.063	157 ± 22
10	184.5	70.6	18	8	0.17 ± 0.060	144 ± 21
11	185.2	71.2	7	5	0.22 ± 0.073	132 ± 30

* Estimate not significant.

current variance thus may relate to large-scale barotropic forcing imposed on the East Siberian Sea through a pressure gradient from the east and/or west.

6. Discussion

We reported velocity and hydrographic observations from the East Siberian Sea to test the hypothesis that the buoyant discharge from the Kolyma River results in an eastward-bound buoyancy-driven coastal current. Using predictions of Yankovsky and Chapman (1997), we expected a surface-advected plume to extend 30–35 km across the gently sloping shelf. This estimate assumes Rossby and Burger numbers of about 0.1 and 0.7, respectively, due to a typical summer discharge of about 10 000 m^3 s^{-1}. Using similar nondimensional and geometric scales, we also expected the coastal current to extend 300–500 km along the shelf (Garvine 1999). The fate of 39 surface drifters deployed into ice-free waters of the Chukchi and East Siberian sea, however, indicated that no such eastward flow was present in the summer of 1995. Instead our drifters described a flow in the opposite direction; that is, the surface circulation in 1995 was westward from the Chukchi into the East Siberian Sea. The 50-day mean flow reached 0.1 m s^{-1} and was statistically significant at the 95% level of confidence. We found little river water on the East Siberian shelf downstream of the Kolyma River. Both velocity and density fields suggested that buoyant river waters did not reach Ayon Island 100 km to the east of the Kolyma River delta. Only in the immediate vicinity of the Kolyma Delta did we find clear evidence of predominantly riverine waters. The absence of an eastward flow requires a reevaluation of the conceptual view of the surface circulation of the East Siberian Sea.

We find large Lagrangian decorrelation scales of about 3 days and 40 km in time and space. The internal deformation radius inshore is 13 km and thus is a factor 3 smaller than the eddy length or spatial decorrelation scale. The square of the ratio between the horizontal scale of the motion L and the internal deformation radius L_D defines a Burger number $S \equiv (L_D/L)^2$ that scales baroclinic vortex tube stretching in the vorticity equation (Pedlosky 1987). In our study area the Burger number is 0.1 inshore and baroclinic vortex tube stretching is weak relative to the diffusion of relative vorticity in the potential vorticity equation. The flow field is linear, though, as the Rossby number $\varepsilon = U/fL \sim 0.005 \ll 1$ is small both inshore and offshore; we here use a velocity scale $U \sim 0.2$ m s^{-1}, a Coriolis parameter $f =$

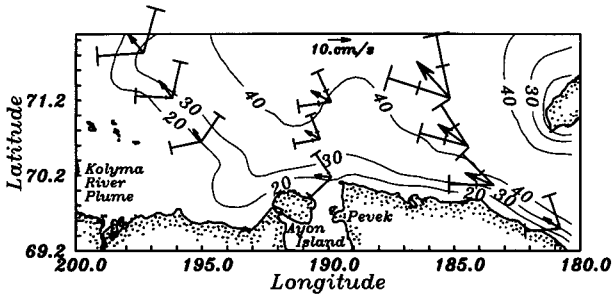

FIG. 18. Map of record mean current vectors for the 1995 ice-free summer season in the East Siberian Sea. The 95% confidence limits for speed and direction are indicated by the lines enclosing each vector. The ticks on these lines represent upper and lower confidence limits for speed while their orientations represent upper and lower confidence limits of direction. The bottom topography is shown also.

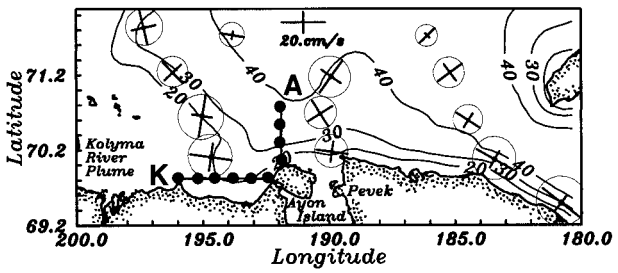

FIG. 19. Map of principal axes of variation. The bottom topography is shown also.

l.4 $\times 10^{-4}$ s^{-1}, and the eddy length scale $L \sim 40$ km. Farther offshore the flow is influenced by the retreat of the ice edge. Here the eddy scale is closer to the local deformation radius (24 km) and the Burger number is about 0.4. While vortex tube stretching is thus still smaller than the diffusion of relative vorticity, the two terms in the vorticity equation are now of the same order of magnitude. The dynamics is not quasigeostrophic, vertical excursions of isopycnals frequently scale with the total water depth.

The northwestward surface circulation is internally consistent with a thermal wind shear associated with the observed sloping isopycnals. The isopycnals outcrop over a scale of about 100 km, that is, the dynamics is not frontal. We interpret our density and velocity observations as the result of an ice edge in retreat. During our study period the ice edge moved northward more than 100 km in less than 2 weeks (0.08 m s^{-1}). In retreat, it leaves melt water behind, which constitutes a line source of buoyancy.

The prevailing westward drift of the surface waters in the East Siberian Sea in 1995 could also be caused by large-scale barotropic and/or baroclinic pressure gradients. Overland and Roach (1987) demonstrate with a barotropic model that a geostrophically controlled northward transport through Bering Strait of the observed magnitude can be driven by a sea level height difference from the Pacific to the Arctic Ocean. Coachman and Rankin (1968) suggest that the highly variable subtidal circulation through Long Strait is caused by different pressures in the Chukchi and East Siberian seas. We speculate that similar pressure gradients could also be imposed from the Laptev Sea in the west through Laptev Strait. The Bering, Chukchi, East Siberian, and Laptev shelf seas each respond to different wind and buoyancy forcing. It is thus conceivable that sloping sea levels result in enhanced flows at the ''choke points'' such as Bering Strait, Long Strait, and Laptev Strait. The dynamical control of transports through these choke points could influence the circulation in both the receiving and the discharging shelf sea. Numerical models that resolve these straits and the internal radius of deformation are needed to investigate the dynamics of the Siberian shelf seas.

Another possible explanation of the interannual variability of the Siberian shelf circulation, we speculate, may relate to decadal-scale climate oscillations. Proshutinsky and Johnson (1997) distinguish two oceanographic circulation regimes that relate to the atmospheric surface pressure distribution in the central Arctic. Following earlier Russian studies (Sokolev 1962), they describe ''cyclonic'' and ''anticyclonic'' regimes that represent oceanic conditions during periods of different interannual atmospheric pressure anomalies over the central Arctic. Our 1995 velocity and salinity observations appear internally consistent with expectation of the ''anticyclonic'' regime of enhanced high pressure systems over the central Arctic. During such years, according to the hypothesis, sea ice cover is much reduced in the East Siberian Sea. Wind-induced motions are postulated to enhance the flushing of ice from this shelf (Sokolov 1962; Proshutinsky and Johnson 1997). In contrast with this theory, however, Maslanik et al. (1996) report reduced ice cover during periods of enhanced cyclone activity off Siberia this decade in what would be the ''cyclonic'' regime. The cause and effect of this interannual variability is thus both unclear and speculative. Overland et al. (1999) argue that decadal-scale oscillations in the Arctic are related to similar oscillations in both the North Pacific (Mantua et al. 1997) and the North Atlantic (Dickson et al. 1997). The linkages between atmospheric forcing, ice cover, buoyancy forcing, shelf circulation, and its impact on the maintenance of the halocline, though tantalizing, are still unsettled.

Acknowledgments. We thank Jackie Grebmeier of the University of Tennessee for the competent deployment of 20 drifters during her expedition to the East Siberian Sea, Steve Sweet for the CTD data collection, and the crew of the R/V *Alpha Helix* for excellent performance under, at times, difficult circumstances. We thank Scott Doluin (University of Tennessee) for assistance with the δ^{18}O measurements. At Rutgers University David Huntley, Hank Statscewich, and Bryan Raynor helped competently with the initial ARGOS retrieval, data processing, and graphics. We are indebted to Richard Garvine of the University of Delaware for positive comments and suggestions that helped to improve the manuscript. The Office of Naval Research (ONR) supported this study through the Arctic Nuclear Waste Assessment Program under Grants N00014-95-1-1158 (AM), N00014-95-1-1215 (TW), N00014-95-F0042, and N000-14-I-1042(LC). TW was also supported by the National Science Foundation Grant OPP-9218756.

REFERENCES

Aagaard, K., and E. C. Carmack, 1989: The role of sea ice and other fresh water in the Arctic circulation. *J. Geophys. Res.*, **94,** 14 485–14 498.

——, L. K. Coachman, and E. C. Carmack, 1981: On the halocline of the Arctic Ocean. *Deep-Sea Res.*, **28,** 529–545.

Bartlett, M. S., 1978: *Stochastic Processes.* 3d ed. Cambridge University Press, 287 pp.

Björk, G., 1989: A one-dimensional time-dependent model for the vertical stratification of the upper Arctic Ocean. *J. Phys. Oceanogr.*, **19,** 52–67.

Carmack, E. C., 1990: Large-scale physical oceanography of polar oceans. *Polar Oceanography, Part A,* W. O. Smith, Ed., Academy Press, 171–222.

Cavalieri, D. J., and S. Martin, 1994: The contribution of Alaskan, Siberian, and Canadian coastal polynyas to the cold halocline layer of the Arctic Ocean. *J. Geophys. Res.*, **99,** 18 343–18 362.

Coachman, L. K., and D. A. Rankin, 1968: Currents in Long Strait, Arctic Ocean. *Arctic,* **21,** 27–38.

——, K. Aagaard, and R. B. Tripp, 1975: *Bering Strait: The Regional Oceanography.* University of Washington Press, 172 pp.

Codispoti, L. A., and F. A. Richards, 1968: Micronutrient distributions

in the East Siberian and Laptev Seas during summer 1963. *Arctic,* **21,** 67–83.
Conquest, R., 1978: *Kolyma: The Arctic Death Camps.* Macmillan, 256 pp.
Cooper, L. W., T. E. Whitledge, J. M. Grebmeier, and T. Weingartner, 1997: The nutrient, salinity, and stable oxygen isotope composition of Bering and Chukchi Seas water in and near Bering Strait. *J. Geophys. Res.,* **102,** 12 563–12 573.
Davis, R. E., 1985: Drifter observations of coastal surface currents during CODE: The statistical and dynamical view. *J. Geophys. Res.,* **90,** 4756–4772.
——, 1991: Observing the general circulation with floats. *Deep-Sea Res.,* **38** (Suppl. 1), S531–S571.
Dickson, R., J. Lazier, J. Meinke, P. Rhines, and J. Swift, 1997: Long-term coordinated changes in the convective activity of the North Atlantic. *Progress in Oceanography,* Vol. 38, Pergamon, 241–295.
Epstein, S., and T. Mayeda, 1953: Variations of O^{18} content of water from natural sources. *Geochim. Cosmochim. Acta,* **42,** 213–224.
Fofonff, N. P., and H. L. Bryden, 1975: Density of sea water. *J. Mar. Res.,* **41,** 69–82.
Garvine, R. W., 1999: Penetration of buoyant coastal discharge onto the continental shelf: A numerical model experiment. *J. Phys. Oceanogr.,* **29,** 1892–1909.
Gawarkiewicz, G. G., and D. C. Chapman, 1995: A numerical study of dense water formation and transport on a shallow, sloping continental shelf. *J. Geophys. Res.,* **100,** 4489–4507.
Grebmeier, J. M, L. W. Cooper, and M. J. DeNiro, 1990: Oxygen isotope composition of bottom seawater and tunicate celluse used as indicators of water masses in the northern Bering and Chukchi seas. *Limnol. Oceanogr.,* **35,** 1182–1195.
Guay, C. K., and K. K. Falkner, 1998: Dissolved barium in Arctic rivers, estuaries, and marginal seas. *Contin. Shelf Res.,* **18,** 859–882.
Jones, E. P., and L. G. Anderson, 1986: On the origin of chemical properties of the Arctic Ocean halocline. *J. Geophys. Res.,* **91,** 10 759–10 767.
Kowalik, Z., and A. Y. Proshutinsky, 1994: The Arctic Ocean tides. *The Polar Oceans and Their Role in Shaping the Global Environment, Geophys. Monogr.,* No. 85, Amer. Geophys. Union, 137–158.
Krauss, W., and C. W. Böning, 1987: Lagrangian properties of eddy fields in the northern North Atlantic as deduced by satellite tracked buoys. *J. Mar. Res.,* **45,** 259–291.
Kundu, P. K., and J. S. Allen, 1976: Some three-dimensional characteristics of low-frequency current fluctuations near the Oregon coast. *J. Phys. Oceanogr.,* **6,** 181–199.
Létolle, R., J. M. Martin, A. J. Thomas, V. V. Gordeev, S. Gusarova, and I. S. Siorov, 1993: ^{18}O abundance and dissolved silicate in the Lena delta and Laptev Sea (Russia). *Mar. Chem.,* **43,** 47–64.
Macdonald, R. W., D. W. Paton, and E. C. Carmack, 1995: The fresh water budget and under-ice spreading of Mackenzie River water in the Canadian Beaufort Sea based on salinity and $^{18}O/^{16}O$ measurements in water and ice. *J. Geophys. Res.,* **100,** 895–919.
Mantua, N. J., S. R. Hare, Y. Zhang, J. M. Wallace, and R. C. Francis, 1997: A Pacific interdecadal climate oscillation with impacts on salmon production. *Bull. Amer. Meteor. Soc.,* **78,** 1069–1079.
Mardia, K. V., 1972: *Statistics of Directional Data.* Academic Press, 357 pp.
Maslanik, J. A., M. C. Serreze, and R. G. Barry, 1996: Recent decrease in Arctic summer ice cover and linkages to atmospheric circulation anomalies. *Geophys. Res. Lett.,* **23,** 1677–1680.
Melling, H., 1993: The formation of a haline shelf front in wintertime in an ice-covered Arctic Sea. *Contin. Shelf Res.,* **13,** 1123–1147.
Middleton, J. F., and C. Garrett, 1986: A kinematic analysis of polarized eddy fields using drifter data. *J. Geophys. Res.,* **91,** 5094–5102.
Milliman, J. D., and R. H. Meade, 1983: World-wide delivery of river sediments to the oceans. *J. Geol.,* **91,** 1–21.
Münchow, A., and R. W. Garvine, 1993: Buoyancy and wind forcing of a coastal current. *J. Mar. Res.,* **51,** 293–322.
——, and E. C. Carmack, 1997: Synoptic flow and density observations near an Arctic shelf break. *J. Phys. Oceanogr.,* **27,** 1402–1419.
Niiler, P. P., A. S. Sybrandy, K. Bi, P. M. Poulain, and D. Bitterman, 1995: Measurements of the water-following capabilities of holey-sock and TRISTAR drifters. *Deep-Sea Res.,* **42,** 1951–1964.
Östlund, H. G., and G. Hut, 1984: Arctic Ocean water mass balance from isotope data. *J. Geophys. Res.,* **89,** 6373–6381.
Overland, J. E., and A. T. Roach, 1987: Northward flow in the Bering and Chukchi Seas. *J. Geophys. Res.,* **92,** 7097–7105.
——, and R. L. Colony, 1994: Geostrophic drag coefficients for the central Arctic derived from Soviet drifting station data. *Tellus,* **46A,** 75–85.
——, J. Miletta Adams, and N. A. Bond, 1999: Decadal variability of the Aleutian low and its relation to high-latitude circulation. *J. Climate,* **12,** 1542–1548.
Paquette, R. G., and R. H. Bourke, 1974: Observations on the coastal current of Arctic Alaska. *J. Mar. Res.,* **32,** 195–207.
——, and ——, 1981: Ocean circulation and fronts related to ice melt-back in the Chukchi Sea. *J. Geophys. Res.,* **86,** 4215–4230.
Pedlosky, J., 1987: *Geophysical Fluid Dynamics.* 2d ed. Springer-Verlag, 710 pp.
Poulain, P.-M., and P. P. Niiler, 1989: Statistical analysis of the surface circulation in the California Current System using satellite tracked drifters. *J. Phys. Oceanogr.,* **19,** 1588–1603.
Proshutinsky, A. Y., and M. A. Johnson, 1997: Two circulation regimes of the wind driven Arctic Ocean. *J. Geophys. Res.,* **102,** 12 493–12 514.
Regier, L., and H. Stommel, 1979: Float trajectories in simple kinematic flows. *Proc. Natl. Acad. Sci.,* **76** (10), 4760–4764; *Geophys. Res.,* **97,** 769–788.
Schlosser, P., D. Bauch, R. Fairbanks, and G. Bönisch, 1994: Arctic river-runoff: Mean residence time on the shelves and in the halocline. *Deep-Sea Res.,* **41,** 1053–1068.
Sokolov, A. L., 1962: Drift of ice in the Arctic Basin and changes in ice conditions over the northern sea route (English transl.), *Probl. Arct. Antarct.,* **11,** j1–j20.
Strain, P. M., and F. C. Tan, 1993: Seasonal evolution of oxygen isotope–salinity relationships in high-latitude surface waters. *J. Geophys. Res.,* **98,** 14 589–14 598.
Sverdrup, H. U., 1929: The waters on the North Siberian shelf. The Norwegian North Polar Expedition with the ''Maud,'' 1918–1925. Scientific Results, Bergen, Norway, Vol. 4, No. 2, 1–133.
Taylor, G. I., 1921: Diffusion by continuous movement. *Proc. London Math. Soc.,* **A20,** 196–211.
U.S. Weather Bureau, 1957: *U.S. Navy Marine Climatic Atlas of the World.* Vol. 6. Arctic Ocean, U.S. Govt. Printing Office, 139 pp.
Vaïkmae, R. A., 1990: Isotope variations in the temperature glaciers of the Eurasian Arctic. *Nucl. Geophys.,* **4,** 45–55.
Weingartner, T., D. J. Cavalieri, K. Aagaard, and Y. Sasaki, 1998: Circulation, dense water formation, and outflow on the northeast Chukchi shelf. *J. Geophys. Res.,* **103,** 7647–7661.
Yankovsky, A. E., and D. C. Chapman, 1997: A simple theory for the fate of buoyant coastal discharges. *J. Phys. Oceanogr.,* **27,** 1386–1401.